Structure
Article

Hydrogen/Deuterium Exchange Analysis of HIV-1 Capsid Assembly and Maturation

Eric B. Monroe,[1,4] Sebyung Kang,[2,4,5] Sampson K. Kyere,[3] Rui Li,[1] and Peter E. Prevelige, Jr.[1,*]
[1]Department of Microbiology
[2]Department of Biochemistry
University of Alabama at Birmingham, Birmingham, AL 35294, USA
[3]Howard Hughes Medical Institute and Department of Chemistry and Biochemistry, University of Maryland Baltimore County, Baltimore, MD 21250, USA
[4]These authors contributed equally to this work
[5]Present address: School of Nano-Biotechnology and Chemical Engineering, Ulsan National Institute of Science and Technology (UNIST), Ulsan Metropolitan City 689-798, Korea
*Correspondence: prevelig@uab.edu
DOI 10.1016/j.str.2010.08.016

SUMMARY

Following budding, HIV-1 virions undergo a maturation process where the Gag polyprotein in the immature virus is cleaved by the viral protease and rearranges to form the mature infectious virion. Despite the wealth of structures of isolated capsid domains and an in vitro-assembled mature lattice, models of the immature lattice do not provide an unambiguous model of capsid-molecule orientation and no structural information is available for the capsid maturation pathway. Here we have applied hydrogen/deuterium exchange mass spectrometry to immature, mature, and mutant Gag particles (CA5) blocked at the final Gag cleavage event to examine the molecular basis of capsid assembly and maturation. Capsid packing arrangements were very similar for all virions, whereas immature and CA5 virions contained an additional intermolecular interaction at the hexameric, 3-fold axis. Additionally, the N-terminal β-hairpin was observed to form as a result of capsid-SP1 cleavage rather than driving maturation as previously postulated.

INTRODUCTION

To become infectious, HIV-1 virions must undergo a maturation process in which an immature virus composed of approximately 5000 molecules of the Gag polyprotein are cleaved by the virally encoded protease (PR) and, subsequently, undergo a striking structural rearrangement to form the mature, infectious virion. Preventing polyprotein cleavage is the mechanism of action of the clinically proven PR inhibitors, and preventing the structural rearrangement following Gag cleavage is the focus of multiple, small molecule, preclinical, development programs (Bartonova et al., 2008; Li et al., 2003; Sticht et al., 2005; Ternois et al., 2005). The enveloped and pleomorphic character of both immature and mature virions has limited structural analysis of intact virus particles by both crystallographic and high-resolution electron microscopic approaches. This, in turn, has hindered drug development efforts. Despite these difficulties, the use of genetic and biochemical tools coupled with a "divide and conquer" approach to the structural biology has led to intermediate resolution structures and models for the immature and mature virions. Although these models have led to hypotheses about the sequence of structural transformations during maturation, there is no direct biochemical evidence to support or refute these hypotheses.

The immature, noninfectious particles are composed of approximately 5000 radially arranged 55 kDa Gag polyprotein molecules with an N-terminal myristoyl group bound to the inner surface of the viral membrane. Gag is composed of the matrix (MA), capsid (CA), and nucleocapsid (NC) principle structural domains. Additionally, short "spacer" peptides connect CA to NC and NC to the "late" domain p6, which is required for viral budding. In the immature virus these are arranged in a manner similar to beads on a string. Following budding, the individual structural components are released by a programmed series of proteolytic cleavage events catalyzed by the virally encoded PR and rearrange to form the mature virion. In the mature virion, MA remains anchored to the interior of the virus envelope, whereas the CA domain collapses to form a conical core that contains NC in complex with a dimer of the genomic RNA.

Because the collapse of CA to form the conical core is required for infectivity, substantial efforts have been made to understand the changes in CA subunit interactions that are coupled to maturation. Structurally, CA consists of stably folded N- and C-terminal domains connected by a flexible linker region. The NTD contains seven α helices, and the N-terminal 13 residues of CA are folded into a β-hairpin structure that can only be formed after cleavage of CA from MA (Kelly et al., 2006) (Figure 1). Targeted mutations have demonstrated that formation of the β-hairpin is required for successful maturation, leading to the suggestion that β-hairpin formation drives rearrangement (Tang et al., 2002; von Schwedler et al., 1998). An extended loop that contains a cyclophilin A (Cyp-A) binding site connects helices 4 and 5, and cyclophilin binding may modulate host cell restriction (Towers et al., 2003). The CTD of HIV CA dimerizes in solution, and this dimerization is thought to play a key role in

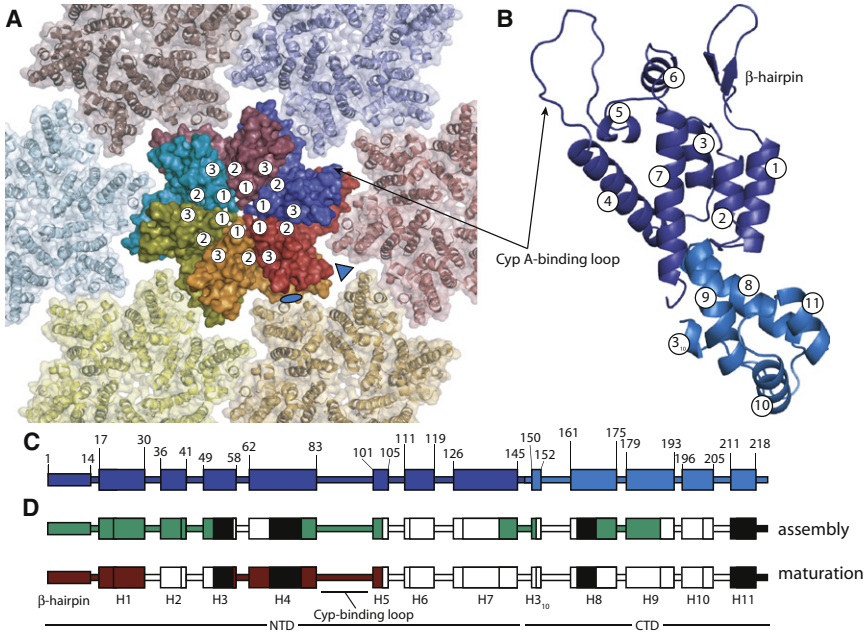

Figure 1. Structures of HIV-1 CA

(A) Top view of assembled HIV-1 CA in a hexameric lattice as produced from the crosslinked crystal structure (Pornillos et al., 2009) (pdb: 3H47). The hexamer is stabilized through H1-H1 and H2-H3 intermolecular interactions, as indicated by the numbered circles in the central, solid hexamer. Adjacent hexamers are presented as cartoons beneath the surface. The 2- and 3-fold interhexamer interfaces are noted by the oval and triangle, respectively.

(B) Cartoon representation of monomeric CA in a mature orientation (Ganser-Pornillos et al., 2007) (pdb: 3DIK) with the β-hairpin, Cyp-A binding loop, and helices labeled. The N-terminal and C-terminal domains are colored as in (C) and Figure 7.

(C) Secondary structure map of CA with amino acid positions of the start and end of each structural element noted using the same numbering system as the peptides used throughout this manuscript.

(D) Secondary structure maps of CA presenting regions in which H/D exchange measurements indicate structural variations that occur during assembly (green) and maturation (red) as colored regions. Those regions in which no variation was observed are white, whereas regions where no data were collected are colored black.

stabilizing both the immature and mature lattices. High-resolution crystallographic structures of the NTD (Gitti et al., 1996; Kelly et al., 2006; Tang et al., 2002), several CTD dimers (Gamble et al., 1997; Ivanov et al., 2007; Kelly et al., 2006; Sticht et al., 2005; Ternois et al., 2005; Worthylake et al., 1999), and recently a complete CA structure have been published (Pornillos et al., 2009). Structural studies in which CA, or its domains, remain tethered to the adjacent domains in the Gag polyprotein revealed little difference in the core fold of the protein, suggesting that changes in the tertiary structure of the NTD and CTD upon maturation are limited to the formation of the N-terminal β-hairpin (Kelly et al., 2006). Recent solid-state NMR studies have also shown that the CA protein structure does not vary significantly between conical and spherical CA assemblies (Han et al., 2010).

Models for the disposition of the CA subunit in the immature and mature virion have been derived from a series of electron microscopic studies and, in the case of the mature lattice, augmented by crystallographic analysis of the fundamental hexameric repeating unit (Briggs et al., 2009; Ganser-Pornillos et al., 2007; Pornillos et al., 2009; Wright et al., 2007). Interactions between an N-terminal myristoyl group and PIP2 as well as electrostatic interactions serve to anchor MA at the inner surface of the envelope. The C terminus of MA is linked to CA via a flexible region. As determined through electron microscopy (EM) studies, the NTD of CA forms a somewhat discontinuous hexameric lattice in the immature virions (Briggs et al., 2009; Wright et al., 2007). The CTD of CA forms dimers that tie the hexamers together. The SP1 peptides from within a hexamer form a bundle underneath the central channel (6-fold axis) of the hexamer. This arrangement serves to tie the CTDs together below the plane of the hexamer, similar to a bouquet of balloons held together by their strings. The NC/RNA complex lies toward the center of the particle and displays no organized symmetry. Although the tomographic reconstructions of the immature lattice have provided insight into the gross organization of the immature Gag/CA lattice, they do not allow for unambiguous docking of the CA crystal structure into the electron densities.

The mature viral core CA is arranged as a hexagonal lattice, similar to the immature lattice, although it is curved into a fullerene cone to form the collapsed core by the inclusion of nonuniformly distributed pentavalent subunits. The interhexamer spacing in the mature lattice is increased to 9.6 nm from the 8.0 nm observed for the immature lattice (Briggs et al., 2004), suggesting that there are alterations in the subunit/subunit interactions. Purified CA can polymerize into tubular and conical forms in vitro, and it has recently been proven possible to crosslink the proteins within these tubes, isolate the hexameric substructures, and solve their crystal structure (Pornillos et al., 2009).

In the mature lattice, the NTD forms a hexameric lattice stabilized by intersubunit NTD/NTD and NTD/CTD interactions. The NTD/NTD interactions involve helices 1, 2, and 3 from each of the six subunits docking to form a bundle surrounding the central pore of the hexamer (Pornillos et al., 2009), as shown in Figure 1. The NTD/CTD interaction is formed when helix 8 of the CTD docks against a region spanning the C terminus of helix 3 through the N terminus of helix 4 from the NTD of the adjacent (counterclockwise) subunit within the same hexamer (Pornillos et al., 2009). Additional contacts are made between helix 11 of the CTD and the C-terminal end of helix 7 in the NTD. Similar to the immature lattice, the individual CA hexamers form a p6 lattice by the dimerization of the C-terminal domain across the local 2-fold axis. The precise molecular interactions associated with this dimerization interface are somewhat unclear. Multiple

crystal and NMR structures of the dimer have been solved, and they display a variety of crossing angles and packing interactions (Gamble et al., 1997; Ivanov et al., 2007; Kelly et al., 2006; Sticht et al., 2005; Ternois et al., 2005; Worthylake et al., 1999).

The divide and conquer approach has focused largely on EM and crystallographic methodologies and has led to the development of a detailed model of the mature CA lattice, whereas the immature lattice is much less well defined. In addition, nearly nothing is currently known regarding the maturation pathway CA follows from the immature lattice to the mature form. Several hypotheses for this maturation process have been proposed, including the disruption of the CA lattice to CA monomers or hexameric units prior to reforming as the mature CA lattice via a de novo assembly or template-guided mechanism in addition to a more conservative, trigger-mediated mechanism (Benjamin et al., 2005; Briggs et al., 2006; Wright et al., 2007).

Because little structural information is currently available to support any maturation model, we have employed hydrogen-deuterium (H/D) exchange mass spectrometry (MS) to refine the structural model of HIV-1 CA assembly and maturation. H/D exchange MS exploits the intrinsic exchange of amide protons with those from solution to examine protein structure and dynamics and has previously been used by our group to detect and characterize the NTD/CTD interaction in the mature CA lattice (Lanman et al., 2003, 2004). Comparative analysis of the protection in unassembled monomeric protein and the immature virion allowed for the identification of contacts formed during assembly (Figure 1D). Comparisons between immature and mature virus-like particles (VLPs) in addition to a mutant blocked at the final CA-SP1 cleavage step illuminated the sequence of conformational rearrangements that occur during the CA maturation process (Figure 1D).

RESULTS

H/D Exchange of MACA and VLPs

Noninfectious HIV-1 immature and mature VLPs were produced by transient transfection of 293T cell lines, and all H/D exchange experiments were performed as described previously (Lanman et al., 2004). Particles trapped at the final cleavage step preceding maturation (CA-SP1) were produced using the CA5 cleavage mutant (Wiegers et al., 1998) cloned into the noninfectious VLP construct. The CA5 mutant carries two mutations at the CA-SP1 junction, one blocking the primary cleavage site, and the other blocking a downstream cryptic cleavage site. The CA-SP1 product of this missed cleavage is frequently termed p25 in contrast to CA, which is often termed p24. Although particles produced by this mutant virus are noninfectious, they display condensed RNA-NC cores and a clear separation of the CA from the viral membrane. It has previously been suggested that these particles probably correspond to a regular maturation intermediate, although it is impossible to rule out a direct effect of the mutations on maturation (Wiegers et al., 1998).

All VLP clones produced particles in sufficient concentrations and with the expected PR-processing pattern as determined by SDS-PAGE (Figure 2). In addition, recombinant MACA protein was prepared as a monomeric, unassembled control. Although the sequence coverage of peptic digests was greater than

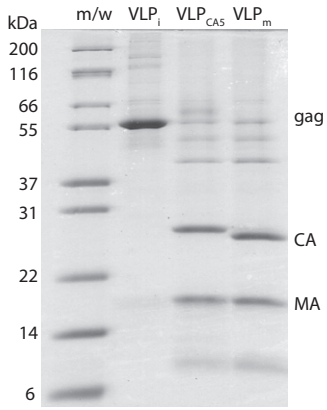

Figure 2. SDS-PAGE Gel of HIV-1 VLPs

Viral particles show the expected cleavage patterns of the structural proteins in the immature (VLP$_i$), CA5 cleavage defect mutant (VLP$_{CA5}$), and mature (VLP$_m$) states. CA-SP1 electrophoreses slightly more slowly than CA due to larger size, although all other components appear similar.

95% in LC-MS/MS experiments, peptides whose signal strength throughout H/D exchange was sufficient for analyses provided ~84% sequence coverage of CA across MACA and the VLPs. No analyzable peptides corresponding to the SP1 region were obtained upon exchange and digestion of VLP$_i$ or VLP$_{CA5}$.

Although details of the H/D exchange data acquisition, reduction, and analysis procedures are described in Experimental Procedures, a brief explanation regarding interpretation may aid in the understanding of the presented results. Briefly, the amount of deuterium incorporated at each exchange time was determined from the corresponding mass spectrum and plotted versus the exchange time. By comparing the exchange profiles for each peptide, regions that become more or less protected may be discerned. The exchange data were fit using nonlinear regression analysis as the sum of three exponentials for kinetic analyses of exchange. This analysis quantifies the number of exchangeable sites in a peptide that exchange at fast ($k > 1\ min^{-1}$), intermediate ($1\ min^{-1} > k > 0.1\ min^{-1}$), or slow ($k < 0.1\ min^{-1}$) rates (Englander and Kallenbach, 1983). The structural implications for these exchange rate constants are such that those with fast exchange rate constants are solvent exposed with no or very weak H-bonding. Amides that exchange within the intermediate range likely contain secondary structural elements, and the exchange rates are driven by transitory conformational fluctuations. Slowly exchanging amides have substantial stability indicative of tertiary and quaternary interactions with stability half-lives of greater than 7 min (for $k = 0.1\ min^{-1}$) versus less than 0.7 min for the fast exchanging amides. Regions of the protein that did not exchange completely during the 48 hr time course of the experiment represent very stable structural elements.

Intermolecular Contacts Formed during Viral Assembly

Comparisons of the peptide exchange profiles of monomeric MACA with those of the immature VLPs allow for the identification of peptides contributing to the intermolecular interactions present in the immature virion. The peptide that spans CA residues 30–40 illustrates the level of protection observed following

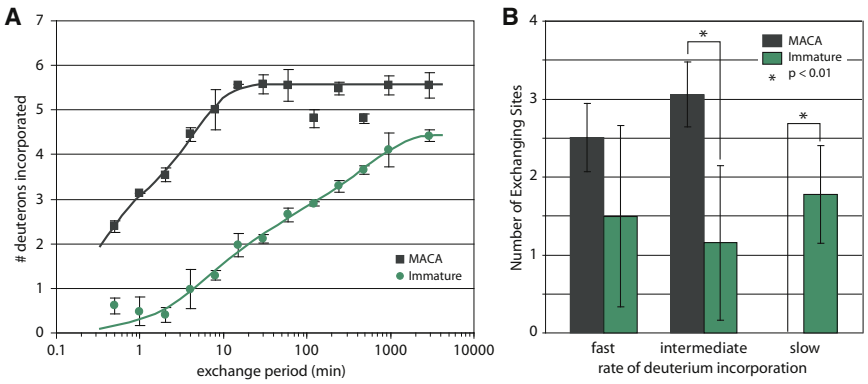

Figure 3. H/D Exchange Plots for the CA Peptide-Spanning Residues 30–40

(A) The exchange plots show increased protection of CA 30–40 upon assembly indicative of the formation of intermolecular contacts in helix 2 in VLP_i (green) compared to the MACA monomeric protein (gray).

(B) Quantitative comparisons of the magnitude of fast, intermediate, and slow exchanging components also illustrate the variation in the exchange patterns with this variation arising in the intermediate and slow exchanging components. Error bars correspond to the standard deviation of deuterium incorporation.

assembly and encompasses five residues of helix 2 as well as the loop between helices 1 and 2. As shown in Figure 3A, the exchange of this peptide is markedly decreased in the immature VLP (green) compared to the monomeric MACA protein (gray). The reduction in both the rate of deuteron incorporation and the total number of deuterons incorporated at long time points (4.5 versus 5.5) is indicative of the formation of intermolecular interactions involving helix 2 upon assembly. Quantitative comparisons of the magnitude of the fast, intermediate, and slow exchanging components similarly illustrate the different nature of the exchange patterns for this peptide (Figure 3B).

Similar increases in protection upon assembly were observed for peptides CA 7–22 (helix 1), CA 23–40 (helices 1 and 2), and CA 41–52 (helices 2 and 3). Collectively, the peptides that span helices 1–3 showed a notable increase in protection following assembly. In accord with previous studies (Lanman et al., 2004), the peptide spanning residues 57–68 of CA, which participates in an intermolecular NTD/CTD interaction in the mature lattice, displayed no change in protection upon assembly because this interaction is absent in both the monomeric MACA protein and the immature virions.

In addition to peptides from the first three helices of CA, the peptide spanning residues 80–103 was more protected in the immature lattice compared to MACA. This peptide encompasses the C-terminal end of helix 4, the cyclophilin-binding loop and helix 5, and lies near the 3-fold axis of the hexameric lattice. These data suggest that some element of the 24 residue long peptide makes contacts in the immature virion that are not present in the unassembled form. The peptide covering residues 169–189 in the CTD of CA showed additional protection following assembly because this peptide includes a significant portion of the interhexameric, dimeric interface (Bartonova et al., 2008; Gamble et al., 1997; Pornillos et al., 2009; Worthylake et al., 1999). Although the exchange data indicates that these regions are involved in assembly, these two peptides will be further discussed when considering maturation.

The regions observed to increase in protection upon assembly are largely consistent with the regions forming inter- and intrahexameric interactions in the mature lattice structure (Ganser-Pornillos et al., 2007; Pornillos et al., 2009), suggesting that the arrangement of CA monomers in the immature lattice is very similar to that in the mature lattice. One exception is the interaction involving the cyclophilin-binding region. This region lies near the 3-fold axis in the mature lattice, but the distance between these 3-fold related regions is too great to allow the maintenance of this interaction in the mature lattice.

Structural Rearrangements Within CA during Viral Maturation

The CA5 Gag cleavage mutant VLP allows us to access the final intermediate on the CA maturation pathway in which the N-terminal domain of CA is cleaved from MA, whereas the C-terminal domain remains attached to the SP1 spacer peptide. By comparing the H/D exchange patterns and rates of immature, CA5, and mature VLPs, the structural aspects of the CA maturation pathway may be interrogated and uncovered.

β-Hairpin Formation

An important question to resolve is whether the β-hairpin forms immediately upon cleavage at the MA-CA junction or whether a subsequent conformational rearrangement is required for its formation. HIV PR-mediated cleavage of Gag in CA5 and mature VLPs alters the pattern of peptide fragments produced upon pepsin digestion. VLP_{CA5} and VLP_m produce a peptide spanning residues 1–22, whereas the corresponding peptide in MACA and VLP_i spans residues 7–22. To compare these peptides we must account for the exchange of residues 1–6 in MACA and VLP_i. Fortunately, residues 1–6 are unstructured in both MACA and VLP_i (Kelly et al., 2006; Tang et al., 2002) and, thus, should exchange at rates >1 min^{-1}, which corresponds to the rapidly exchanging component of the multi-exponential fits. To allow comparison, the fits for the observed exchange patterns of CA 7–22 from MACA and VLP_i were adjusted by including the rapid exchange of six additional residues (corresponding to residues CA 1–6) (Figure 4A). The adjusted exchange profiles show an increase in protection at long time points for all three forms of VLPs relative to unassembled MACA protein, suggestive of the formation of intersubunit interactions. The hairpin that spans residues 1–16 is unformed in the immature virus localizing the protection to residues 17–22, which form the N terminus of helix 1. Strikingly, at short time points there is a statistically significant difference in the extent of protection between mature virions (VLP_m) and the immature or partially matured virions (VLP_i, VLP_{CA5}), as shown in Figure 4B. We attribute this difference to exchange protection afforded by the formation of the β-hairpin structure. The exchange profiles for VLP_i and VLP_{CA5} are nearly identical at early time points, suggesting that the N terminus of CA in

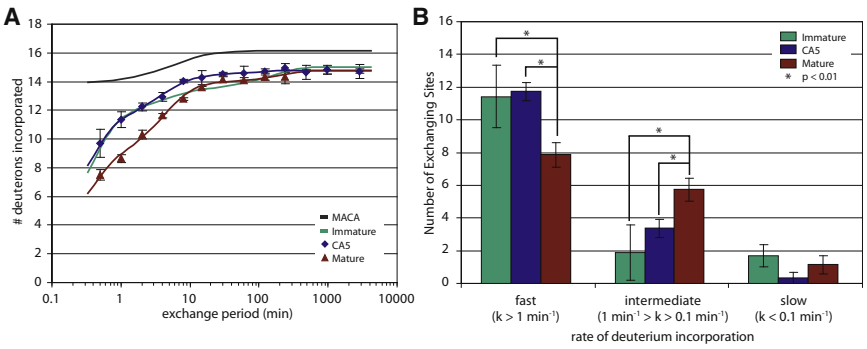

Figure 4. H/D Exchange Plots for the Peptide-Spanning the N-Terminal β-Hairpin

(A) Exchange plots for VLP_{CA5} (blue) and VLP_i (green, corrected for rapid exchange of residues 1–6) appear identical, whereas the VLP_m (red) shows slightly increased protection from exchange as afforded by the β-hairpin. All VLPs show increased protection over MACA (gray, corrected for rapid exchange of residues 1–6).

(B) Quantitative analysis of the exchange data supports this interpretation with a significant ($p < 0.01$) difference in the magnitude of the fast and intermediate components present between VLP_i/VLP_{CA5} and VLP_m. Error bars correspond to the standard deviation of deuterium incorporation.

VLP_{CA5} is unstructured, and the β-hairpin is not formed prior to cleavage of SP1 from CA.

Helices 1–3

Overlapping peptides provide a mechanism to increase the resolution of H/D exchange experiments. The presence of overlapping peptides, CA 23–40 and CA 30–40, allows us to localize the variation in exchange pattern to residues 23–29, which lie in helix 1. The exchange profiles for CA 30–40 (helix 2) were similar across the VLPs, meaning that the changes seen in CA 23–40 (Figure 5) arise from residues 23–29. The loss of protection in VLP_{CA5} relative to the immature and mature forms suggests a disruption of the packing of helix 1 in the partially mature state with minimal perturbation of interactions involving helices 2 and 3. Slight variations in the exchange profiles of VLP_i and VLP_m suggest that helix 1 may have slightly different packing interactions in the immature versus mature states.

NTD-CTD and CTD-CTD Interactions

Another hallmark of CA maturation is the formation of an NTD-CTD intersubunit, intrahexamer interaction in which helix 8 in the CTD is packed against the C terminus of NTD helix 3, the intervening loop, and the N terminus of helix 4 from the adjacent CA monomer in the hexamer (Lanman et al., 2004; Pornillos et al., 2009). The NTD portion of this interacting surface is represented in the exchange experiments by a peptide spanning residues 57–68. As previously reported, this peptide exchanges in a bimodal manner with one population being protected and corresponding to those molecules present in the collapsed, mature core and the other exchanging rapidly and excluded from the core (Lanman et al., 2004). However, this peptide rapidly exchanged in VLP_i and VLP_{CA5} (see Figure S1 available online), indicating that the NTD/CTD interaction is not yet formed. This result is in accord with the suggestion that cleavage of the CA-SP1 junction is necessary to allow the CTD to move upward and dock with adjacent NTDs.

The portion of the CTD involved in the mature NTD-CTD interaction is included in the peptide that spans residues 169–189. This peptide also contains the CTD-CTD interhexamer contact, which occurs along the 2-fold axis. This peptide displays protection upon assembly, yet is similarly protected in both the VLP_i and VLP_m forms. Because we would expect increased protection in the mature form due to the formation of the NTD-CTD interface, the basis for the similar protection patterns in the mature and immature forms is not obvious, although several possible explanations exist. The crystal structure of the mature hexamer suggests that the dimer interface is somewhat flexible and plastic (Pornillos et al., 2009), and multiple docking models have been proposed (Byeon et al., 2009; Ganser-Pornillos et al., 2007). One possible explanation is that the CTD-CTD interface remodels during maturation, resulting in equivalent protection in both VLP_m and VLP_i. Alternatively, it is possible that the stabilization afforded by CTD dimerization masks any increased protection arising from the formation of the NTD-CTD interaction. Unfortunately, the current data provide no basis to distinguish between these two interpretations.

Helix 4 and Cyclophilin-Binding Loop

The crystal structure of the mature HIV hexamer shows considerable flexibility in the region of the cyclophilin-binding loop

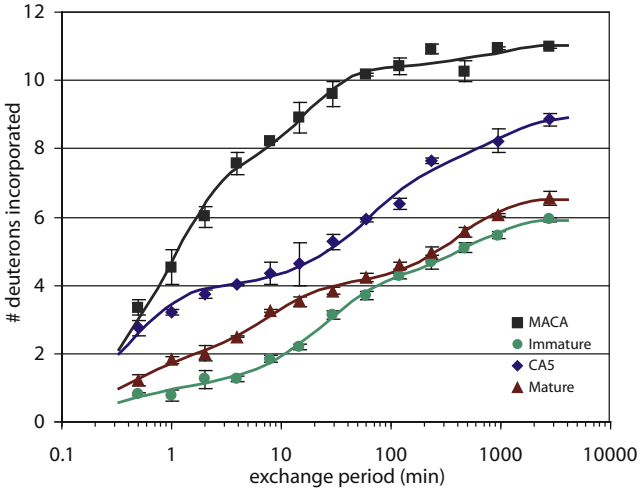

Figure 5. H/D Exchange Plots for the Peptide-Spanning CA Residues 23–40

All assembled forms—VLP_i (green), VLP_{CA5} (blue), and VLP_m (red)—show increased protection relative to MACA (gray). VLP_i shows the most protection of all three assembled forms. No differences in exchange behavior between the assembled forms was observed for an overlapping peptide spanning CA residues 30–40, thus localizing the changes to CA 23–29, which resides solely within helix 1. The increased exchange of VLP_{CA5} (relative to VLP_i and VLP_m) is suggestive of a transition state between two orientations of helix 1. Error bars correspond to the standard deviation of deuterium incorporation.

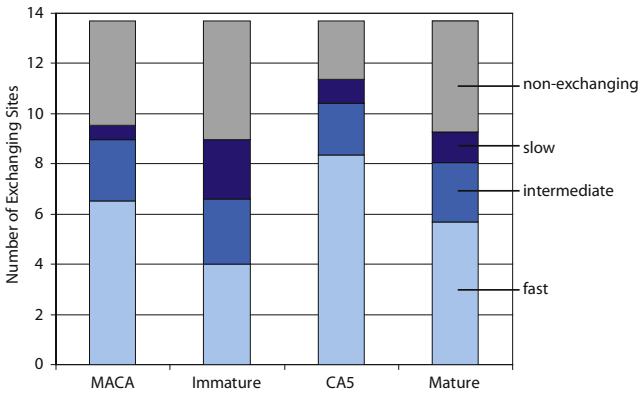

Figure 6. Reduced H/D Exchange Data for the Peptide-Spanning CA Residues 80–103

The number of rapidly exchanging amide protons (light blue, $k > 1\ min^{-1}$) was markedly decreased in the immature VLPs compared to MACA and mature VLPs. CA5 VLPs had more rapidly exchanging amide protons than all other forms. The number of amides exchanging at intermediate (blue, $1\ min^{-1} > k > 0.1\ min^{-1}$) and slow rates (dark blue, $k < 0.01\ min^{-1}$) did not notably vary across the VLPs. The decrease in the protons that did not exchange during the time period of the experiments (gray) in the CA5 VLPs indicates that this region undergoes considerable strain during maturation.

(residues 84–97). In the exchange experiments, this region is represented by a peptide spanning residues 80–103, which shows no variation in protection between the mature VLP and the MACA protein. In the mature HIV lattice, this region lies at a local 3-fold, and no interactions between the loops have been detected. As previously discussed, this peptide displays increased protection in the immature form suggestive of an intersubunit interaction. The structurally related region in N-MLV forms a 3-fold interaction in the immature lattice, but this interaction is abolished upon maturation (Mortuza et al., 2008). Tomographic EM reconstructions of the immature CA lattice (Briggs et al., 2009; Wright et al., 2007) are not of sufficient resolution to observe such an interaction, but all show a density present at the 3-fold axis.

Strikingly, in VLP_{CA5} this peptide presented a significantly increased number of rapidly exchanging amide protons compared to the other VLPs ($p < 0.01$) or monomeric MACA ($p < 0.003$) (Figure 6). We interpret this as a result of strain-induced hydrogen bond breaking in this region, likely in or around helix 5, during the transition from the immature to mature CA lattice. The simplest mechanism to generate the strain would be preservation of the 3-fold interaction, while the NTD moves toward the mature conformation. Following SP1 cleavage, the 3-fold interaction would be abolished as a result of the upward movement of the CTD to form the NTD/CTD interaction. The upward translation of the CTD would also serve to increase the interhexameric spacing in the mature lattice relative to the immature lattice (Ganser-Pornillos et al., 2007; Pornillos et al., 2009).

DISCUSSION

From the results of the H/D exchange experiments, we have developed a model of HIV-1 maturation that is consistent with previously reported biochemical and structural studies and provides insight into aspects of the HIV-1 assembly and maturation pathways that have been inaccessible to more traditional techniques.

Comparisons of the exchange patterns of the immature virus to those of the monomeric protein (MACA) and the mature virus indicate that the protected regions in the immature virus correspond quite closely to those in the mature virus, suggesting very similar NTD-CA packing arrangements and intermolecular interactions in both immature and mature virions. There is excellent correspondence between the regions that become protected upon assembly and the intersubunit interfaces seen in the crystal structure of CA hexamers (Pornillos et al., 2009). A recent report by Briggs et al. (2009) presents a model of the immature lattice based on cryoEM tomographic reconstructions with a notably different monomer packing arrangement than that of the mature hexamers presented by Pornillos et al. (2009). The subunit interfaces presented in the Briggs model appear inconsistent with the protection patterns that we observe by H/D exchange MS.

The primary changes to the exchange patterns from the immature to the mature virus include: (1) an increase in protection in the region forming the β-hairpin in mature virions, (2) a slight increase in exchange in helix 1, (3) a decrease in protection around the CypA-binding loop at the 3-fold symmetric axis, and (4) protection of the mature NTD/CTD interface. Based on these observations, we suggest that the structural changes that occur over the course of HIV-1 CA maturation are the formation of the N-terminal β-hairpin, a slight reorientation of helix 1, the dissolution of a 3-fold interaction involving the region around the CypA-binding loop, and the formation of the NTD/CTD interface.

The addition of H/D exchange data from the CA5 structural intermediate allows for the examination of the maturation pathway as it progresses from the immature to mature states. Although maturation is a dynamic event in vivo, by blocking the final cleavage event in the Gag maturation pathway, the CA5 intermediate presents a trapped, static representation of a presumptive transient structural intermediate. While this exact state does not exist along the normal maturation pathway, CA-SP1 does present a natural kinetic bottleneck in maturing virions owing to the greatly reduced rate of PR-mediated cleavage (Pettit et al., 1994). In this regard, the CA5 VLPs allow for the interrogation of a transitional state between immature and mature virions.

Notably, the exchange data suggest that the N-terminal β-hairpin has not yet formed in CA5, nor has the mature NTD-CTD interaction. No large-scale structural changes were indicated by the exchange profiles of any peptide other than the lack of the N-terminal β-hairpin. However, a slight, generalized reduction in protection was observed for peptides from the NTD in the CA5 structural intermediate, while no such difference was observed in the exchange rates of peptides from the CTD. The increased exchange of the NTD of CA in VLP_{CA5} suggests that the cleavage of MA from CA initiates motion of helix 1 at the center of the hexamer, whereas the 3-fold interaction around the Cyp-A binding loop appears to be maintained, although in a strained conformation.

EM images of immature and mature HIV particles both contain a layer of regular density attributable to CA (Briggs et al., 2009;

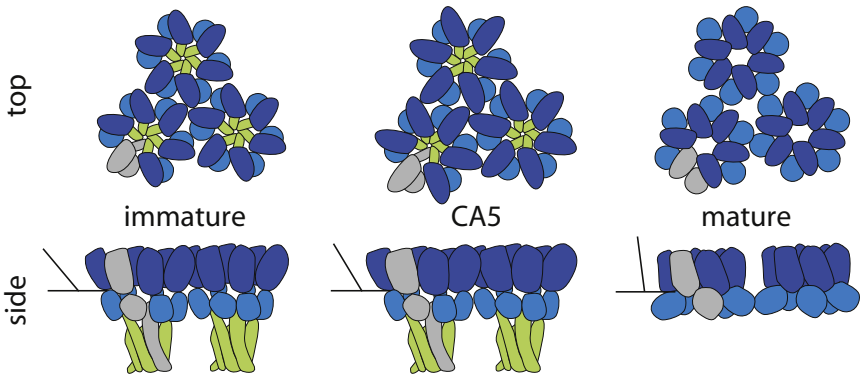

Figure 7. Schematic Model of HIV-1 CA Maturation

The model of HIV-1 CA assembly and maturation with the NTD and CTD colored as in Figures 1B and 1C. The immature hexameric lattice (left) assembles with a set of intermolecular interactions nearly identical to the mature form (right) minus the features indicative of maturation (N-terminal β-hairpin and NTD-CTD intrahexameric interaction), although an additional interface along the 3-fold axis appears in the immature form. The NTD (dark blue) and CTD (light blue) of CA are held in a vertical orientation by SP1 (green) in both the immature and CA5 states (a single monomer is also shown in gray). Following MA-CA cleavage, the NTD appears to be strained in the CA5 state as the 3-fold interface is maintained, whereas H1 (at the opposite side of the monomer) reorients toward its mature orientation. After CA-SP1 cleavage, the CTD is able to rotate to its mature orientation and form the NTD-CTD interface and the N-terminal β-hairpin forms. Taken together, maturation appears to occur by the remodeling of several intermolecular interfaces but does not require the disassembly of the individual hexamers.

Ganser-Pornillos et al., 2007; Wright et al., 2007), and a similar layer is also present in CA5 HIV particles (Wiegers et al., 1998). Although the fact that only approximately half of the CA subunits are incorporated into the mature core suggests that some dissociation of the CA lattice to substructures likely occurs, the continued presence of the CA lattice and similar H/D exchange patterns for the vast majority of the CA peptides suggest that maturation proceeds to the point of CA-SP1 cleavage without gross disassembly of the CA lattice. There is currently no way to interrogate the state of the transient intermediates between CA-SP1 cleavage and the mature form. Although dissociation of the lattice to monomeric CA subunits followed by de novo CA assembly is a potential maturation pathway, we prefer a more conservative pathway. The similarity in the protection patterns in the immature, CA5, and mature forms, coupled with the high protein CA concentration within the particle, which promotes subunit association, leads us to favor a model in which maturation proceeds through partial lattice disruption and intersubunit remodeling rather than via complete dissociation and reassembly. There is ample precedent in viruses as diverse as polio, polyoma, herpes, and the bacteriophage for CA assembly from preformed pentamers and hexamers (Palmenberg, 1982; Salunke et al., 1989; Tonegawa and Hayashi, 1970; Xie and Hendrix, 1995) as well as maturation through intersubunit remodeling without dissociation (Conway et al., 2001; Jiang et al., 2003; Trus et al., 1996).

The results from the H/D exchange experiments are consistent with the previously proposed model of HIV maturation in which the two domains of CA rearrange through rigid body motion without gross refolding of CA subunits (Wright et al., 2007). In our model of maturation (Figure 7), cleavage of MA from CA primes and initiates the rotation of the NTD toward its mature conformation, while the 3-fold interaction is maintained by exploiting the structural plasticity of the NTD. Following CA-SP1 cleavage, the CTDs are free to rotate from their position largely below the NTD (Wright et al., 2007) to a position that enables the formation of the intrahexameric, intersubunit NTD-CTD interaction in the mature CA lattice (Lanman et al., 2004). This motion of the CTDs may also remodel the CTD-CTD interhexamer interface along the 2-fold axis. These motions would provide a means to alter the interhexamer distance, as observed between immature and mature lattices (Briggs et al., 2004).

Additionally, because the data indicate that the N-terminal β-hairpin forms following CA-SP1 cleavage, hairpin formation may serve as a mechanism to lock helix 1 in its mature orientation and restrict further NTD motion. It has previously been proposed that formation of the β-hairpin occurs immediately following cleavage of MA from CA and could serve to drive maturation (Tang et al., 2002; von Schwedler et al., 1998). Our results suggest that this is not the case and that rather β-hairpin formation is a consequence of maturation.

EXPERIMENTAL PROCEDURES

Preparation of HIV-1 VLPs

In order to reduce the biohazard of working with intact HIV-1 virions, VLPs were produced from noninfectious, modified pNL4-3 provirus plasmids as previously described (Lanman et al., 2004). Briefly, a four-base deletion in *env* results in premature termination of *env* translation, resulting in the production of a nonfunctional env protein that is secreted and not incorporated into budding particles. In addition a 109 codon deletion in *pol*, which results in the inactivation of RT and IN, was incorporated from the disabled HXB2 provirus plasmid pFN to form the plasmid $pVLP_m$. An additional point mutation, D24N, in PR was incorporated to inactivate PR to produce $pVLP_i$ and enables the production of immature VLPs containing full-length, unprocessed Gag protein. To produce $pVLP_{CA5}$, previously reported CA5 point mutations at the CA-SP1 cleavage site and a cryptic cleavage site in SP1 (Wiegers et al., 1998) were cassette cloned into the $pVLP_m$ construct.

VLPs were produced for H/D exchange experiments by transiently transfecting 293T cells with $pVLP_i$, $pVLP_{CA5}$, or $pVLP_m$ with FuGene 6 (Roche, Indianapolis, IN, USA). Cells were incubated for 8 hr in the presence of the plasmid and FuGene 6 prior to removal of the media and replenishment with serum-free media to reduce interference from serum components during mass spectrometric analysis. Following ~48 hr of expression, the media were collected, and cellular debris was removed by centrifugation and filtration through a 0.45 μm syringe filter. VLPs were then collected via centrifugation through a 20% sucrose cushion and resuspended in PBS. The amount of produced VLPs and the extent of proteolysis were estimated by SDS-PAGE.

Preparation of MACA Protein

MACA derived from the HIV infectious clone pNL4-3 with a C-terminal His_6 tag was subcloned into a dual expression vector with the yeast N-terminal myristyl transferase (yNMT) gene, both under the control of an inducible *lac* promoter (Tang et al., 2002) and transformed into BL21 (DE3) codon plus RIL competent

cells (Stratagene, La Jolla, CA, USA). Protein expression was then induced with 1 mM IPTG for 5 hr. The cells were harvested and lysed, clarified by centrifugation, and purified with cobalt affinity and ion exchange chromatography. The mass of purified MACA was confirmed by MS.

H/D Exchange

H/D exchange experiments were performed largely as previously described (Kang and Prevelige, 2005; Lanman et al., 2004). Exchange was initiated by diluting MACA or the VLPs 10-fold into deuterated phosphate buffer (equivalent pH = 7). This exchange reaction was allowed to progress at 20°C for 30 s, 1, 2, 4, 8, 15, or 30 min, 1, 2, 4, 8, 16, or 48 hr prior to quenching the reaction by adjusting the pH to 2.5 with formic acid (final concentration 1%) and immediately flash freezing the quenched sample in liquid nitrogen. Samples were then stored at −80°C prior to MS analysis.

For MS analysis, samples were rapidly thawed and mixed with pepsin (~10 μM final concentration) and digested on ice for 2 min. Digested samples (~50 pmol CA) were desalted and marginally separated on a C4 trap (Microm, Auburn, CA, USA). The 20 μl injection loop, C4 trap, and all tubing were kept submerged in an ice bath to minimize back exchange. Digested peptides were rapidly eluted from the C4 trap with a 5%–95% ACN gradient (50 μl/min, with 0.1% formic acid) and electrosprayed into a hybrid ion trap-FT ICR mass spectrometer (LTQ-FT, Thermo Finnigan, Waltham, MA, USA). Eluted, exchanged peptides were identified via exact mass measurements with the 7T FT-ICR MS for H/D exchange experiments based on peptide identifications determined by MS/MS sequencing of non-exchanged peptides.

Data Processing

The level of deuterium incorporation was determined by calculating the centroid from the isotopic distribution for each peptide with the Deuterator software package (Pascal et al., 2007). Exchange plots were then plotted for the measured values of deuteron incorporation versus time. Exchange plots for each peptide detected in this study are presented in Figures S2–S5. By comparing the maximal exchange values for numerous peptides, back exchange was estimated at ~20%. The exchange profiles were fit in SigmaPlot (Systat, San Jose, CA, USA) to a sum of three exponentials derived from the exchange rate expression (Englander and Kallenbach, 1983):

$$D = N - A * \exp(-k_1 t) - B * \exp(-k_2 t) - C * \exp(-k_3 t), \quad (1)$$

where D is the observed number of deuterons incorporated at time t, and N is the total number of protons that exchanged within the time domains of the experiment. A, B, and C correspond to the number of exchangeable sites that are observed to exchange with a rate constant k_1 (fast, >1.0 min^{-1}), k_2 (intermediate, 0.01–1.0 min^{-1}), or k_3 (slow, <0.01 min^{-1}), respectively. The regression values for the number of exchangeable sites that exchange with each binned rate constant and the associated standard error calculated from the fits were used to calculate a p value via a two-tailed *t* test. The number of exchangeable sites as determined by the peptide length subtracting the N terminus and the number of prolines and multiplying this value by 90% (percentage of deuterium in exchange solution) was also calculated. The magnitude of a fourth exchange rate bin was then calculated by subtracting the sum of the detected exchangeable sites (A, B, and C) from the total number of exchangeable sites. This provides a value of "non-exchanging" amides, which consists of both sites that exchange at rates lower than the time scale of this experiment as well as deuterons lost to back exchange. The level of back exchange was estimated at ~20% and is uniform across the samples and peptides, regardless of peptide length or composition. As such, increases in the number of "non-exchanging" amides are interpreted as indicative of the formation of very stable interactions.

SUPPLEMENTAL INFORMATION

Supplemental Information includes five figures and can be found with this article online at doi:10.1016/j.str.2010.08.016.

ACKNOWLEDGMENTS

The authors would like to thank Matthew Renfrow for assistance with the mass spectrometer, Terje Dokland and Michael Spilman for electron microscopy assistance, and Hans-Georg Krausslich for the gift of the CA5 plasmid. This work was supported by NIH grant R01AI044626 to P.E.P., R37AI30917 to Michael F. Summers, and fellowship support to E.B.M. (F32GM087994) and S.K.K. (F31GM076979).

Received: May 24, 2010
Revised: August 11, 2010
Accepted: August 13, 2010
Published: November 9, 2010

REFERENCES

Bartonova, V., Igonet, S., Sticht, J., Glass, B., Habermann, A., Vaney, M.C., Sehr, P., Lewis, J., Rey, F.A., and Krausslich, H.G. (2008). Residues in the HIV-1 capsid assembly inhibitor binding site are essential for maintaining the assembly-competent quaternary structure of the capsid protein. J. Biol. Chem. *283*, 32024–32033.

Benjamin, J., Ganser-Pornillos, B.K., Tivol, W.F., Sundquist, W.I., and Jensen, G.J. (2005). Three-dimensional structure of HIV-1 virus-like particles by electron cryotomography. J. Mol. Biol. *346*, 577–588.

Briggs, J.A., Simon, M.N., Gross, I., Krausslich, H.G., Fuller, S.D., Vogt, V.M., and Johnson, M.C. (2004). The stoichiometry of Gag protein in HIV-1. Nat. Struct. Mol. Biol. *11*, 672–675.

Briggs, J.A., Grunewald, K., Glass, B., Forster, F., Krausslich, H.G., and Fuller, S.D. (2006). The mechanism of HIV-1 core assembly: insights from three-dimensional reconstructions of authentic virions. Structure *14*, 15–20.

Briggs, J.A., Riches, J.D., Glass, B., Bartonova, V., Zanetti, G., and Krausslich, H.G. (2009). Structure and assembly of immature HIV. Proc. Natl. Acad. Sci. USA *106*, 11090–11095.

Byeon, I.J., Meng, X., Jung, J., Zhao, G., Yang, R., Ahn, J., Shi, J., Concel, J., Aiken, C., Zhang, P., and Gronenborn, A.M. (2009). Structural convergence between Cryo-EM and NMR reveals intersubunit interactions critical for HIV-1 capsid function. Cell *139*, 780–790.

Conway, J.F., Wikoff, W.R., Cheng, N., Duda, R.L., Hendrix, R.W., Johnson, J.E., and Steven, A.C. (2001). Virus maturation involving large subunit rotations and local refolding. Science *292*, 744–748.

Englander, S.W., and Kallenbach, N.R. (1983). Hydrogen exchange and structural dynamics of proteins and nucleic acids. Q. Rev. Biophys. *16*, 521–655.

Gamble, T.R., Yoo, S., Vajdos, F.F., von Schwedler, U.K., Worthylake, D.K., Wang, H., McCutcheon, J.P., Sundquist, W.I., and Hill, C.P. (1997). Structure of the carboxyl-terminal dimerization domain of the HIV-1 capsid protein. Science *278*, 849–853.

Ganser-Pornillos, B.K., Cheng, A., and Yeager, M. (2007). Structure of full-length HIV-1 CA: a model for the mature capsid lattice. Cell *131*, 70–79.

Gitti, R.K., Lee, B.M., Walker, J., Summers, M.F., Yoo, S., and Sundquist, W.I. (1996). Structure of the amino-terminal core domain of the HIV-1 capsid protein. Science *273*, 231–235.

Han, Y., Ahn, J., Concel, J., Byeon, I.J., Gronenborn, A.M., Yang, J., and Polenova, T. (2010). Solid-state NMR studies of HIV-1 capsid protein assemblies. J. Am. Chem. Soc. *132*, 1976–1987.

Ivanov, D., Tsodikov, O.V., Kasanov, J., Ellenberger, T., Wagner, G., and Collins, T. (2007). Domain-swapped dimerization of the HIV-1 capsid C-terminal domain. Proc. Natl. Acad. Sci. USA *104*, 4353–4358.

Jiang, W., Li, Z., Zhang, Z., Baker, M.L., Prevelige, P.E., Jr., and Chiu, W. (2003). Coat protein fold and maturation transition of bacteriophage P22 seen at subnanometer resolutions. Nat. Struct. Biol. *10*, 131–135.

Kang, S., and Prevelige, P.E., Jr. (2005). Domain study of bacteriophage p22 coat protein and characterization of the capsid lattice transformation by hydrogen/deuterium exchange. J. Mol. Biol. *347*, 935–948.

Kelly, B.N., Howard, B.R., Wang, H., Robinson, H., Sundquist, W.I., and Hill, C.P. (2006). Implications for viral capsid assembly from crystal structures of HIV-1 Gag(1-278) and CA(N)(133-278). Biochemistry *45*, 11257–11266.

Lanman, J., Lam, T.T., Barnes, S., Sakalian, M., Emmett, M.R., Marshall, A.G., and Prevelige, P.E., Jr. (2003). Identification of novel interactions in HIV-1

capsid protein assembly by high-resolution mass spectrometry. J. Mol. Biol. *325*, 759–772.

Lanman, J., Lam, T.T., Emmett, M.R., Marshall, A.G., Sakalian, M., and Prevelige, P.E., Jr. (2004). Key interactions in HIV-1 maturation identified by hydrogen-deuterium exchange. Nat. Struct. Mol. Biol. *11*, 676–677.

Li, F., Goila-Gaur, R., Salzwedel, K., Kilgore, N.R., Reddick, M., Matallana, C., Castillo, A., Zoumplis, D., Martin, D.E., Orenstein, J.M., et al. (2003). PA-457: a potent HIV inhibitor that disrupts core condensation by targeting a late step in Gag processing. Proc. Natl. Acad. Sci. USA *100*, 13555–13560.

Mortuza, G.B., Dodding, M.P., Goldstone, D.C., Haire, L.F., Stoye, J.P., and Taylor, I.A. (2008). Structure of B-MLV capsid amino-terminal domain reveals key features of viral tropism, gag assembly and core formation. J. Mol. Biol. *376*, 1493–1508.

Palmenberg, A.C. (1982). In vitro synthesis and assembly of picornaviral capsid intermediate structures. J. Virol. *44*, 900–906.

Pascal, B.D., Chalmers, M.J., Busby, S.A., Mader, C.C., Southern, M.R., Tsinoremas, N.F., and Griffin, P.R. (2007). The Deuterator: software for the determination of backbone amide deuterium levels from H/D exchange MS data. BMC Bioinformatics *8*, 156.

Pettit, S.C., Moody, M.D., Wehbie, R.S., Kaplan, A.H., Nantermet, P.V., Klein, C.A., and Swanstrom, R. (1994). The p2 domain of human immunodeficiency virus type 1 Gag regulates sequential proteolytic processing and is required to produce fully infectious virions. J. Virol. *68*, 8017–8027.

Pornillos, O., Ganser-Pornillos, B.K., Kelly, B.N., Hua, Y., Whitby, F.G., Stout, C.D., Sundquist, W.I., Hill, C.P., and Yeager, M. (2009). X-ray structures of the hexameric building block of the HIV capsid. Cell *137*, 1282–1292.

Salunke, D.M., Caspar, D.L., and Garcea, R.L. (1989). Polymorphism in the assembly of polyomavirus capsid protein VP1. Biophys. J. *56*, 887–900.

Sticht, J., Humbert, M., Findlow, S., Bodem, J., Muller, B., Dietrich, U., Werner, J., and Krausslich, H.G. (2005). A peptide inhibitor of HIV-1 assembly in vitro. Nat. Struct. Mol. Biol. *12*, 671–677.

Tang, C., Ndassa, Y., and Summers, M.F. (2002). Structure of the N-terminal 283-residue fragment of the immature HIV-1 Gag polyprotein. Nat. Struct. Biol. *9*, 537–543.

Ternois, F., Sticht, J., Duquerroy, S., Krausslich, H.G., and Rey, F.A. (2005). The HIV-1 capsid protein C-terminal domain in complex with a virus assembly inhibitor. Nat. Struct. Mol. Biol. *12*, 678–682.

Tonegawa, S., and Hayashi, M. (1970). Intermediates in the assembly of phi X174. J. Mol. Biol. *48*, 219–242.

Towers, G.J., Hatziioannou, T., Cowan, S., Goff, S.P., Luban, J., and Bieniasz, P.D. (2003). Cyclophilin A modulates the sensitivity of HIV-1 to host restriction factors. Nat. Med. *9*, 1138–1143.

Trus, B.L., Booy, F.P., Newcomb, W.W., Brown, J.C., Homa, F.L., Thomsen, D.R., and Steven, A.C. (1996). The herpes simplex virus procapsid: structure, conformational changes upon maturation, and roles of the triplex proteins VP19c and VP23 in assembly. J. Mol. Biol. *263*, 447–462.

von Schwedler, U.K., Stemmler, T.L., Klishko, V.Y., Li, S., Albertine, K.H., Davis, D.R., and Sundquist, W.I. (1998). Proteolytic refolding of the HIV-1 capsid protein amino-terminus facilitates viral core assembly. EMBO J. *17*, 1555–1568.

Wiegers, K., Rutter, G., Kottler, H., Tessmer, U., Hohenberg, H., and Krausslich, H.G. (1998). Sequential steps in human immunodeficiency virus particle maturation revealed by alterations of individual Gag polyprotein cleavage sites. J. Virol. *72*, 2846–2854.

Worthylake, D.K., Wang, H., Yoo, S., Sundquist, W.I., and Hill, C.P. (1999). Structures of the HIV-1 capsid protein dimerization domain at 2.6 A resolution. Acta Crystallogr. D Biol. Crystallogr. *55*, 85–92.

Wright, E.R., Schooler, J.B., Ding, H.J., Kieffer, C., Fillmore, C., Sundquist, W.I., and Jensen, G.J. (2007). Electron cryotomography of immature HIV-1 virions reveals the structure of the CA and SP1 Gag shells. EMBO J. *26*, 2218–2226.

Xie, Z., and Hendrix, R.W. (1995). Assembly in vitro of bacteriophage HK97 proheads. J. Mol. Biol. *253*, 74–85.